# Transition of Nanostructure in DNA−Cationic Surfactant Complexes with the Added Salt

Tatsuya Kawashima, Akihiko Sasaki, and Shigeo Sasaki*

*Department of Chemistry, Faculty of Sciences, Kyushu University, 33 Hakozaki, Higashi ku, Fukuoka 812, Japan*

*Received January 19, 2006; Revised Manuscript Received April 2, 2006*

Nanostructures of complexes of DNA with single-chain surfactant of octadecyltrimethylammonium (OTA) and double-chain surfactant of didodecyldimethylammonium (DDA) in aqueous NaCl solution at concentration, $C_s$, from 0 to 500 mM were studied using small-angle-scattering techniques (SAXS). SAXS profiles of the DNA−OTA complex show two SAXS peaks with a spacing ratio of $1:3^{1/2}$ in the solution at $C_s$ below 150 mM and three peaks with a spacing ratio of $1:3^{1/2}:4^{1/2}$ at $C_s$ above 250 mM. Contents of $Na^+$ and $Cl^-$ ions in the complexes evaluated from the atomic absorbance for $Na^+$ and the potentiometry for $Cl^-$ revealed charge molar ratios of OTA/DNA = 1 and DDA/DNA = 1.25. Contents of $Na^+$ and $Cl^-$ ions per ionic unit of DNA molecule in the DNA−OTA complex equilibrating with the solution at $C_s$ below 100 mM were much less than 0.1, while they increased with NaCl concentration at $C_s$ above 200 mM. The DNA−OTA complex in the solution at $C_s$ above 260 mM exhibited an endothermic peak in the DSC measurements, and the others did not. On the basis of the experimental results, the salt concentration dependent nanostructures are discussed.

## 1. Introduction

The gene carrier mechanism and the efficient transfection to biological cells remain a fascinating challenge for the near future.[1] The mechanism to induce the more compact state of colossal genomic DNA molecules within the small confines of the cell nucleus, the bacterial cytoplasm, and viral capsid is a key subject to be investigated. The biologically relevant DNA condensing agents are cationic proteins (e.g., histone) and multivalent polyamines such as spermidine and spermine.[2−5] The electrostatic interaction between anionic DNA and multivalent cationic entities plays an important role in inducing the compact state of DNA. The multivalent micelles composed of the cationic surfactant molecules concentrated in the vicinity of the DNA molecule are also able to pack DNA in an ordered manner to form crystallized structures such as 2D hexagonal and lamella, which can be determined from the characteristic peaks in the small-angle X-ray scattering (SAXS) profiles.[6] The 2D hexagonal structure for complexes of DNA with cetyltrimethylammonium bromide has been confirmed on the basis of the first two diffraction peaks with a spacing ratio of $1:3^{1/2}$.[7] A multilamellar structure was found in complexes formed by DNA with a double-chained surfactant of dioctadecyldimethylammonium bromide.[8] The SAXS profiles obtained by Safinya et al. for the DNA complexes with the mixture of ionic and neutral double-chained surfactant have revealed that the lattice spacings of DNA molecules in the complexes depend on the ratio of the surfactants[9] and the salt concentration.[10] It has been found that the lattice spacing of the surfactant bilayer and DNA molecule increases with an increase of the neutral surfactant in the mixture and/or an increase of the salt concentration. The increase of the neutral surfactant decreases the net charge density of the bilayer, and the salt shields and weakens the electrostatic interaction between DNA and the bilayer. The electrostatic interaction among ionic entities plays very important roles in the architecture of the DNA−surfactant complexes.

The electrostatic interaction between the ionized flexible polymer and the surfactant molecules plays an essential role in constructing the nanostructures of the polyelctrolyte surfactant complex molecules (PSC), in which the surfactant micelles are concentrated in the vicinity of polyelectrolyte chain and form the liquid crystal structure. We have demonstrated that an addition of salt molecules to the PSC increases the lattice spacing to induce the order−disorder transition at the salt concentration about a few hundred millimolar.[11] The highly flexible chains of vinyl polymers can be distributed according to the intricate crystal structures of surfactant micelles,[12−14] but the rigid chain such as DNA cannot. Due to the constrained force of DNA, the cubic crystal is rarely found in the structures of the double-stranded DNA−surfactant complexes. The SAXS profiles characteristic of the 2D hexagonal have been observed for the complexes of DNA with the single-chain surfactant.[15] The 2D hexagonal structure has been explained by two controversial models, hexagonal arrays of rod micelles and DNA[15] and a hexagonal array of DNA surrounded by the inverse micelles[6] as shown in Figure 1. The SAXS profiles of equimolar complex of DNA and surfactant molecule have exhibited two peaks with a spacing ratio of $1:3^{1/2}$, although the SAXS profiles of the complex containing excess surfactant have shown three peaks with a spacing ratio of $1:3^{1/2}:4^{1/2}$.[6] The present investigation is aimed at clarifying roles that the electrostatic interaction plays in forming the structures indicated by the discrepant profiles mentioned above. The SAXS profiles of the complexes of DNA with the double-chain surfactants[6,9,10,16] have been identified as multilamellar structures with alternating bilayers and DNA monolayers. The lattice spacings of surfactant lamellar and DNA sandwiched between lamella layers have been found to strongly depend on a molar ratio of the surfactant to DNA, a charge density of the surfactant bilayer, and the salt concentration.[10] Our interests here are how the electrostatic interaction works in constructing the lamellar structures. In the present investigation, the SAXS profiles were obtained for the complexes of DNA with single-chain surfactant of octadecyltrim-

* s-sskscc@mbox.nc.kyushu-u.ac.jp.

10.1021/bm060059j CCC: $33.50 
Published on Web 05/19/2006

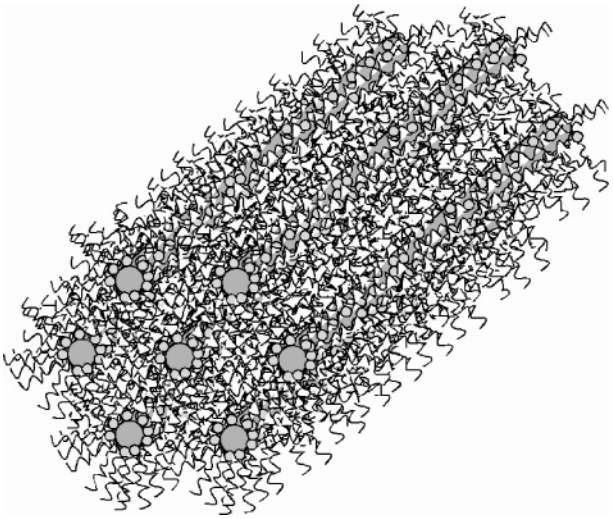

**Figure 1.** Schematic model of 2D hexagonal DNA-inverted surfactant complex.

ethylammonium (OTA) and double-chain surfactant of didodecyldimethylammonium (DDA) in the aqueous NaCl solution at concentration, $C_s$, from 0 to 500 mM. In the SAXS profiles for the DNA−OTA complex, two peaks with a spacing ratio of $1:3^{1/2}$ were observed at $C_s$ below 150 mM and three peaks with a spacing ratio of $1:3^{1/2}:4^{1/2}$ were observed at $C_s$ above 250 mM. The contents of $Na^+$ and $Cl^-$ ions in the complexes were evaluated by using the atomic absorbance technique for $Na^+$ and the potentiometry for $Cl^-$. A difference between $Na^+$ and $Cl^-$ contents in the DNA−OTA complex was very small, although a molar ratio of the excess amount of $Cl^-$ over $Na^+$ per ionic unit of DNA molecule in the DNA−DDA complex was more than 0.25. Molar ratios of $Na^+$ and $Cl^-$ ions to an ionic unit of DNA molecule in the DNA−OTA complex in the solution at $C_s$ below 100 mM were much less than 0.1, while they increased with $C_s$ at $C_s$ above 200 mM. The DNA−OTA complex in the solution at $C_s$ above 260 mM exhibited an endothermic peak in the DSC measurements, and the others did not. On the basis of the experimental results described above, the salt concentration dependent nanostructures are discussed.

## 2. Experimental Section

**2.1. Materials.** The DNA−OTA or DNA−DDA complexes were prepared by mixing equal amounts (typically 20 mL) of 30 mM (phosphate group unit) DNA solution and 30 mM octadecyltrimethylammonium chloride (OTAC) or 30 mM didodecyldimethylammonium chloride (DDAC) solution. The complex formed as the white aggregate after shaking for 24 h at a room temperature were filtered, rinsed thoroughly with water (more than 500 mL), dried in a vacuum, and stored. It should be mentioned that surfactant concentrations much higher than cmc (0.3 mM for OTAC[17] and 0.2 mM for DDAC[18]) are not needed to form the complex of surfactants with DNA. The surfactant molecules are concentrated to form micelles near a DNA molecule and complex with DNA because of the strong electrostatic attraction between them. A given weight of the dried complex, $w_{complex}$ (typically 0.1 g) was immersed in a given volume of the aqueous NaCl solution, $V_{NaCl}$ (typically 50 mL).

The suspension containing the complex was shaken thoroughly for more than a week to equilibrate with the NaCl solution. The SAXS experiments were carried out for the complexes suspended in the aqueous solutions. To increase the mole ratio of the surfactant to DNA in the DNA−OTA complex for the SAXS experiment, a given amount of OTAC was added to the suspension.

DDAC was obtained by ion-exchanging the didodecyldimethylammonium bromide (DDAB) with HCl. DNA from salmon testes was purchased from Sigma and used without further purification. All the chemicals were of reagent grade.

**2.2. Small-Angle X-ray Scattering.** The SAXS measurements for the complex equilibrating with the NaCl solution were made with a SAXS spectrometer of BL45XU installed at SPring8 of Japan Synchrotron Radiation Research Institute, Hyogo, Japan. The scattering vectors, $q = (4\pi/\lambda)\sin\theta/2$, where $\lambda$ was a wavelength of the beam ($\lambda = 0.09$ nm) and $\theta$ a scattering angle ($\theta = 0.08-5°$), ranged from 0.1 to 6 $nm^{-1}$. The temperature dependence of SAXS profiles was obtained with controlling temperature within 0.1 °C.

**2.3. Quantitative Analysis of $Na^+$, $Cl^-$, and DNA in the Complex.** The concentration of DNA diffused into the NaCl solution from the complex, [$DNA^{out}$], was determined from the optical density at 260 nm ($\epsilon = 6.17 \times 10^6$ $mol^{-1}$ $cm^2$) measured by an UV spectrometer (Ubest-50, Jasco). A diffusing amount of DNA from the complex to the solution phase was evaluated from a value of [$DNA^{out}$] as described later.

The amounts of $Na^+$ and $Cl^-$ in the complex were obtained as follows. A part of the complex equilibrating with the NaCl solution was filtered out, weighed ($w^{H_2O_2}_{complex}(C_s)$) and then immersed into a given volume of 20% $H_2O_2$ solution, $V_{H_2O_2}$ (typically 30 mL), to be oxidized and decomposed at 80 °C. The decomposition in the suspension was judged from the loss of turbidity. It took two weeks at most to decompose the organic entities of complex in the oxidative solution. The concentration of $Cl^-$ was measured with the chloride selectivity electrode (9617B, Thermo Orion Inc., U.S.A.), and the concentration of $Na^+$ was measured with atomic adsorption (AA-625-11, Simadzu, Japan) at a wavelength 589 nm. Calibrations of the chloride selectivity electrode were carried out for the aqueous NaCl solutions containing 10% $H_2O_2$, since the $H_2O_2$ content in the decomposed solution was estimated to be between 10% and 20% from the contents of organic entities. It should be mentioned that the difference between the calibration curves for the solutions containing 10% and 20% $H_2O_2$ was negligibly small. The electric potentials obtained for the $H_2O_2$ solutions were, however, about 10% higher than those for the ordinary solutions. The molar amounts of $Na^+$ and $Cl^-$ in the decomposed complex, $N'_{Na^+}$ and $N'_{Cl^-}$were obtained from the concentrations of $Na^+$ and $Cl^-$ in the decomposed solutions, [$Na^+$] and [$Cl^-$] by using the relations $N'_{Na^+} = [Na^+] \times V_{H_2O_2}$ and $N'_{Cl^-} = [Cl^-] \times V_{H_2O_2}$. The molar ratio of the surfactant to an ionic unit of DNA in the dried complex, $\rho$ ($\equiv N^0_{surfactant}/N^0_{DNA}$; $N^0_{surfactant}$ and $N^0_{DNA}$ are molar amounts of the surfactant and the ionic group of DNA in the dried complex) can be obtained from the molar amount of $Cl^-$ in the dried complex, $N^0_{Cl^-}$, using the relation

$$\rho = (308.5 + M_{surfactant})N^0_{Cl^-}/[w^{dry}_{complex} - N^0_{Cl^-}(M_{surfactant} + 35.5)] + 1 \quad (1)$$

where $w^{dry}_{complex}$ is a weight of the dried complex. Here, $M_{surfactant}$ is a molecular weight of the surfactant ($M_{OTA} = 312.6$ and $M_{DDA} = 400$), and a molecular weight of an ionic unit of DNA is assumed to be 308.5. It should be noted that the contents of $Na^+$ ion in the dried complexes of DNA−OTA and DNA−DDA are assumed to be null in eq 1. This was experimentally confirmed as shown in section 3.2. The values of $\rho$ obtained for the DNA−OTA and DNA−DDA complexes, respectively, were $1.00 \pm 0.06$ and $1.25 \pm 0.06$. The molar amounts of $Na^+$ and $Cl^-$ in the complex, $N_{Na^+}$ and $N_{Cl^-}$, were given by $N_{Na^+} = N'_{Na^+}\eta$ and $N_{Cl^-} = N'_{Cl^-}\eta$ where $\eta = w_{complex}[308.5 + M_{surfactant}\rho]/[(w^{H_2O_2}_{complex}(C_s) - 23N'_{Na^+} - 35.5N'_{Cl^-})(308.5 + M^{\rho}_{surfactant} + 35.5(\rho - 1))]$. The molar amount of ionic unit of DNA in the complex equilibrating with the NaCl solution, $N_{DNA}$, was obtained from the following relation:

$$N_{DNA} = w_{complex}/\{308.5 + M_{surfactant}\rho + 35.5(\rho - 1)\} - [DNA^{out}] \times V_{NaCl} \quad (2)$$

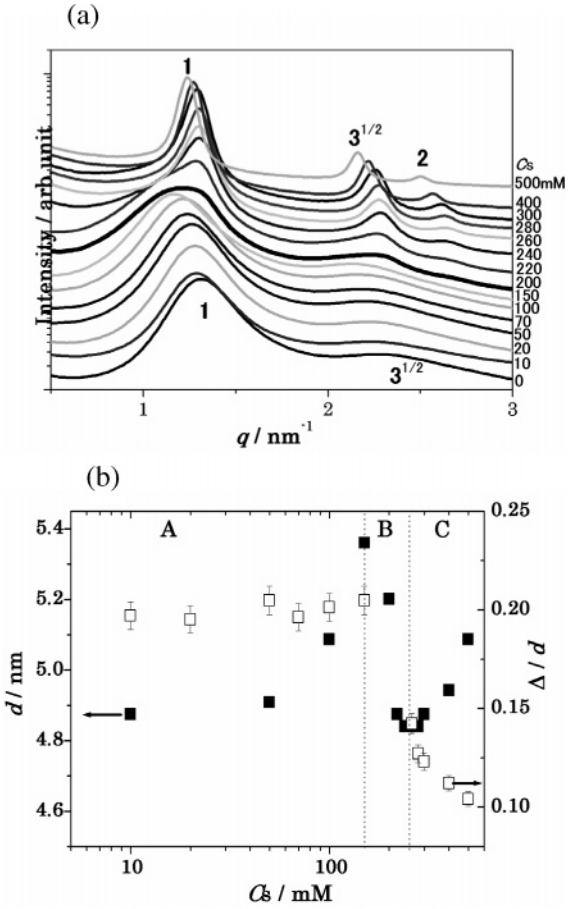


**Figure 2.** SAXS profiles of DNA−OTA complex in the aqueous NaCl solutions (a) and salt concentration dependence of the lattice constants ($d$), and the parameter of disorder, ($\Delta/d$) obtained from the first peak of SAXS profiles (b). (a) Peaks with the spacing ratios of $1:3^{1/2}$ and $1:3^{1/2}:2$, respectively, are observed in the profiles of the complex at $C_s$ below 150 mM and above 250 mM. (b) The closed and opened symbols, respectively, are the lattice spacing and the parameter of disorder. Three regions A, B, and C partitioned by two vertical dotted lines are the defect hexagonal, transition, and ordinary hexagonal regimes.

**2.4. Differential Scanning Calorimetry.** The differential scanning calorimetry, DSC, measurements were carried out with a DSC 120 calorimeter (Seiko Inc., Japan) at a heating rate of 0.5 °C/min. The complex equilibrating with the NaCl solution was taken out and weighed ($w^{DSC}_{complex}$) after wiping out the water attached to the complex. The complex was put into an aluminum pan together with about 50 $\mu$L of the NaCl solution for the DSC measurement. The transition enthalpy per 1 g complex, $\Delta H_{measure}$, was obtained from an integration area of the DSC curve and $w^{DSC}_{complex}$. The transition enthalpy per 1 mol surfactant, $\Delta H$, was obtained from the $\Delta H_{measure}$ using the following relation:

$$\Delta H = \Delta H_{measure} \times \chi \times M_{surfactant} \quad (3)$$

where $\chi$ is given by

$$\chi = (N_{DNA} + N_{Cl^-} - N_{Na^+})/[308.5N_{DNA} + 23N_{Na^+} + 35.5N_{Cl^-} + M_{surfactant}(N_{DNA} + N_{Cl^-} - N_{Na^+})] \quad (3-a)$$

## 3. Results

**3.1. Nanostructures of the Complexes.** Figure 2 shows the SAXS profiles and the lattice spacing of the DNA−OTA complexes in the solutions at salt concentrations from 0 to 500 mM. The values of lattice spacing, $d$, shown in Figure 2b are obtained from the relation $d = 2\pi/q_1$, where $q_1$ is a $q$-value of the first peak (a peak at the lowest $q$) shown in Figure 2a. The complexes in the solutions at salt concentrations, $C_s$, below 150 mM emerge as two broad peaks with a ratio of $1:3^{1/2}$, while the complex in the solution at $C_s$ above 250 mM emerges as three peaks with a ratio of $1:3^{1/2}:2$ as shown in Figure 2a. The scattering intensity of the $i$th peak, $I_i(q)$, can be approximately described by the Gaussian function as follows:

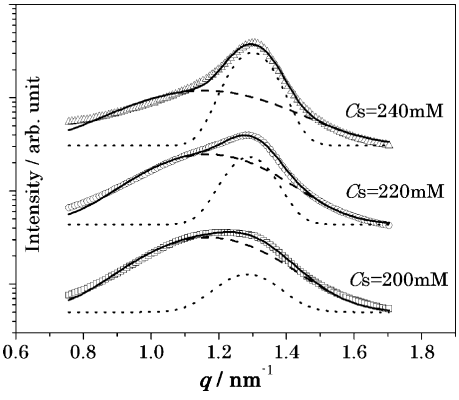


**Figure 3.** SAXS profiles of DNA−OTA complex in the solutions at $C_s$ = 200, 220, and 240 mM. The profiles can be decomposed to two Gaussian curves represented by the broken and dotted lines. The solid lines represent the curves best fitted to the data.

$$I_i(q) = I_{i0} + \frac{2A_i}{w_i\sqrt{\pi/2}} \exp\left(\frac{-2(q-q_i)^2}{w_i^2}\right) \quad (4)$$

where $q_i$, $w_i$, $A_i$, and $I_{i0}$, respectively, are a scattering vector of the $i$th peak, the half-width of $q$, the integrated intensity, and the background. The $w_i$ value can be a measure of the degree of disorder of the scattering plane. The structural parameter of disorder $\Delta_i/d$, defined as $\Delta_i/d \equiv \sqrt{w_i d/\pi^3}$,[19] is estimated and shown in Figure 2b. There exist three $C_s$ regimes characterized by the nanostructures of DNA−OTA complexes. The regimes will be denoted as a defect hexagonal regime at $C_s$ below 200 mM, an ordinary hexagonal regime at $C_s$ above 260 mM, and a transition regime at $C_s$ between 200 and 260 mM. The two peaks with the spacing ratio $1:3^{1/2}$ are observed in the defect hexagonal regime, while three peaks with the spacing ratio $1:3^{1/2}:2$ are in the ordinary hexagonal regime. The lattice spacing $d$ increases with $C_s$ in both the defect and ordinary hexagonal regimes as shown in Figure 2b. This indicates that the compaction of DNA is loosened with an increase in $C_s$. The structural parameter of disorder $\Delta_i/d$ in the ordinary hexagonal regime decreases with the increase of $C_s$, but it is invariant in the defect hexagonal regime. This suggests that the domain size of ordered structures in the complex increases with the increase of $C_s$ in the ordinary hexagonal regime and that the addition of salt induces no change of the domain size fluctuation of ordered structures in the defect hexagonal regime. The transition regime is the region in which two types of structures coexist. The main SAXS peaks emerging from the complexes at $C_s$ = 200, 220, and 240 mM shown in Figure 2a can be regarded as a sum of two peaks. The decomposition is successfully made by best fitting the function $I_1(q) = I_{10} + \sum_{i=1,2} 2A_i/w_i\sqrt{\pi/2} \exp[-2(q - q_i)^2/w_i^2]$ to the peaks as shown in Figure 3, and the obtained parameters are tabulated in Table 1. It should be mentioned that the values of $q_1$ and $q_2$, respectively, are very close to the $q$-values of the first peaks at $C_s$ = 150 and 260 mM. An intensity ratio of the peak at $q = q_1$ to the sum of peak intensities at $q$

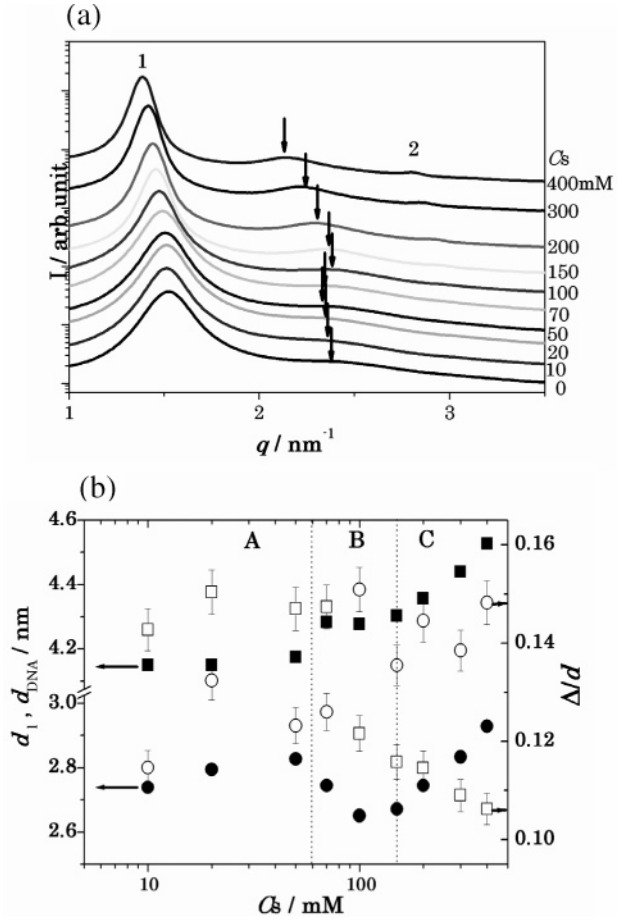


**Figure 4.** SAXS profiles of DNA−DDA complex in aqueous NaCl solutions (a) and NaCl concentration dependence of the lattice constants ($d$), and the parameter of disorder, ($\Delta/d$) obtained from the first peak of SAXS profiles (b). (a) Broad peaks with a spacing ratio of 1:2 as denoted by 1 and 2 are scattered from the multilamellar lattice of surfactant bilayers. The peaks indicated by arrows are scattered from the ordered array of DNA between the surfactant bilayers. (b) Closed squares and open squares, respectively, are $d_{DDA}$ and $\Delta/d$ obtained from the first peak of the SAXS profiles. Closed circles and open circles represent the spacing of DNA, $d_{DNA}$, and $\Delta/d$ obtained from the peak assigned to the DNA−DNA spacing in SAXS profiles. Three regions A, B, and C partitioned by two vertical dotted lines are the undulated lamella, transition lamella, and ordinary lamella regimes.

**Table 1.** Fitting Results[a] of Salt Concentration Dependent Peak Positions ($q_1$, $q_2$), Peak Widths ($w_1$, $w_2$), and Relative Intensity of the First Peak [$A_1/(A_1 + A_2)$] for the Observed Profiles at $C_s$ from 150 to 260 mM

| $C_s$ | 150 mM | 200 mM | 220 mM | 240 mM | 260 mM |
|---|---|---|---|---|---|
| $q_1$/nm$^{-1}$ | 1.17 | 1.17 | 1.17 | 1.16 | |
| $w_1$/nm$^{-1}$ | 0.21 | 0.34 | 0.35 | 0.42 | |
| $q_2$/nm$^{-1}$ | | 1.29 | 1.29 | 1.30 | 1.30 |
| $w_2$/nm$^{-1}$ | | 0.17 | 0.13 | 0.13 | 0.14 |
| $A_1/(A_1 + A_2)$ | 1 | 0.88 | 0.74 | 0.52 | 0 |

[a] The best fitting curves at the transition regime ($C_s$ = 200−240 mM) are shown in Figure 3.

$= q_1$ and $q_2$, $A_1/(A_1 + A_2)$ gradually decreases from 0.88 to 0.52 with an increase in $C_s$ from 200 to 240 mM as shown in Table 1. These facts indicate that the structure existing in the complex at $C_s$ = 150 mM vanishes and that the other structure existing in the complex at $C_s$ = 260 mM grows with the increase of $C_s$ in the transition regime.

Figure 4a,b show the $C_s$ dependence of the SAXS profiles, the lattice spacing, and the parameter of disorder obtained for the DNA−DDA complex. The peaks with a spacing ratio 1:2

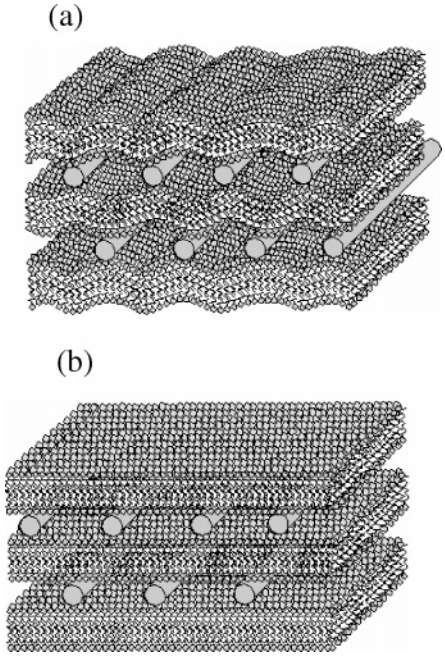


**Figure 5.** Possible schematic models of undulated multilamellar structure (a) and ordinary flat lamellar structure (b).

emerged from the multilamella lattice of bilayers of DDA give the lattice spacing, $d_L$, which can be estimated from the relation, $d_L = 2\pi/q_1$, where $q_1$ is a scattering vector of the first peak. A weak peak observed between the peaks mentioned above is due to the correlation length of DNA arraying between the lamellas, $d_{DNA} = 2\pi/q_{DNA}$, where $q_{DNA}$ is a scattering vector of the peak sandwiched in two lamella peaks. The measured value of $d_L$ monotonically increases with $C_s$ in the $C_s$ range above 60 mM, but it is invariant with $C_s$ at $C_s$ below 60 mM as shown in Figure 4b. This indicates that the shielding effect of salt on the attraction between DNA and the DDA bilayer is effective at $C_s$ above 60 mM but not at $C_s$ below 60 mM. The $C_s$ dependence of $d_{DNA}$ shown in Figure 4b can be classified into three regimes of $C_s$, below 60 mM, between 60 and 150 mM, and above 150 mM. The value of $d_{DNA}$ is substantially invariant with $C_s$ in the first regime, decreases with $C_s$ in the second regime, and increases with $C_s$ in the third regime. This is different from the $C_s$ dependence of $d_L$. The value of $d_{DNA}$ is determined by the force balance between the attraction between DNA and the DDA bilayers and the repulsion between DNA molecules sandwiched between the DDA bilayers. The subtle force balance inducing the rather sophisticated $C_s$ dependence of $d_{DNA}$ might be related to the fluctuations of the structures that can be inferred from the structural parameters of disorder. The structural parameters of disorder, $\Delta_i/d$ for the lamella and the DNA array are estimated by fitting the function described by eq 4 to the peak. The obtained results are plotted against $C_s$ and shown in Figure 4b. In the whole region of $C_s$, the $\Delta/d_{DNA}$ is substantially invariant with $C_s$. The $\Delta/d_L$ decreases with $C_s$ in the second regime and the third regime, while it is invariant with $C_s$ in the first regime. The structure in the first regime is inferred to be rather rigid from the fact that the values of $d_L$, $d_{DNA}$, $\Delta/d_L$, and $\Delta/d_{DNA}$ are substantially invariant despite an increase of the shielding effect of salt molecules on the electrostatic interaction. The strong attraction between anionic DNA and cationic sheets bends to make the sheets closer with each other at the low $C_s$. The strong hydration of headgroups of DDA molecules repels the sheets at a DNA free region[16] and undulates lamella sheets as shown in Figure 5a. The first regime will be denoted an undulated lamella regime. The decrease of $\Delta/d_L$ with $C_s$ in the third regime

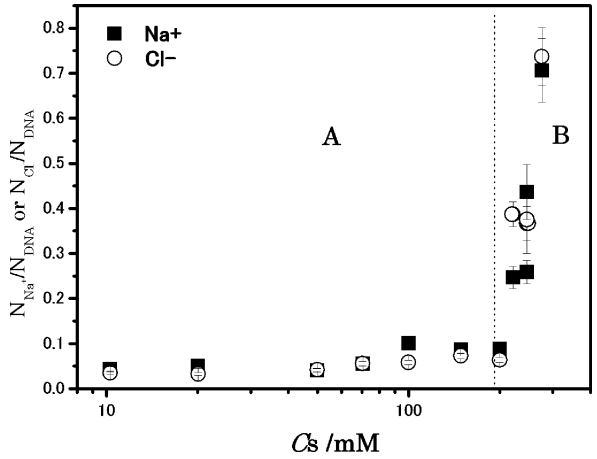


**Figure 6.** Contents of $Na^+$ and $Cl^-$ ions per ionic unit of DNA in the DNA−OTA complex as functions of the salt concentration. Two regions A and B partitioned by a vertical dotted line are the defect hexagonal and transition regimes.

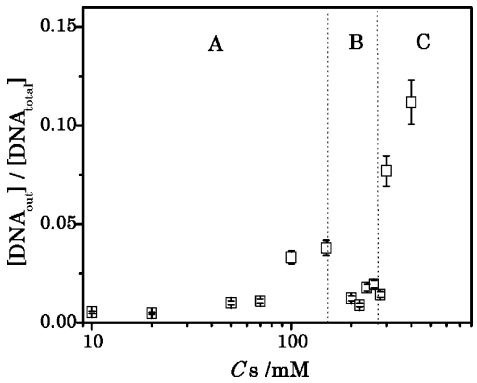


**Figure 7.** Salt concentration dependence of DNA amount diffusing from the DNA−OTA complex to the NaCl solution equilibrating with the complex. Three regions A, B, and C partitioned by two vertical dotted lines are the defect hexagonal, transition, and ordinary hexagonal regimes.

shown in Figure 4b suggests a less undulated structure of lamellar sheets. Accordingly, the third regime will be denoted an ordinary lamella regime. The second regime between the undulated lamella regime and the ordinary lamella regime will be denoted a transition regime.

**3.2. Quantities of $Na^+$, $Cl^-$, and DNA in the DNA−Surfactant Complex.** Figure 6 shows quantity ratios of $Na^+$ and $Cl^-$ ions to an ionic unit of DNA in the DNA−OTA complex equilibrating with the NaCl solution, $N_{Na^+}/N_{DNA}$ and $N_{Cl^-}/N_{DNA}$ as functions of $C_s$. It should be mentioned that the quantitative analysis of $Na^+$ and $Cl^-$ ions of the complex in the ordinary hexagonal regime could not be made because of soft and fragile properties of the complex in this regime. It is obvious from Figure 6 that the difference between amounts of $Na^+$ and $Cl^-$ ions contained in the complex is null within experimental error. One OTA molecule pairs to an ionic unit of DNA molecule in the complex to satisfy the electrical neutrality condition. Figure 6 also shows that the amounts of $Na^+$ and $Cl^-$ in the complex increase with $C_s$ in the transition regime.

A small amount of DNA molecules diffuses from the DNA−OTA complex into 50 mL of the NaCl solution that is equilibrating with 0.1 g of the complex. Figure 7 shows an amount of DNA molecules diffusing from the complex to the NaCl solution, $[DNA^{out}] \times V_{NaCl}/(N_{DNA} + [DNA^{out}] \times V_{NaCl})$ as a function of $C_s$. The diffusing amount of DNA increases

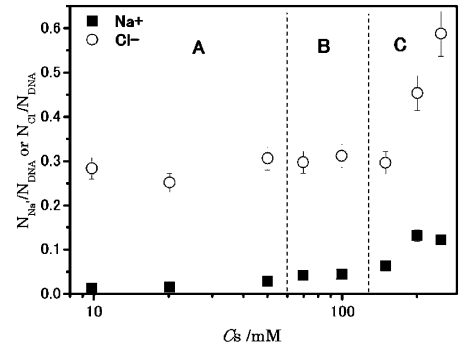


**Figure 8.** Salt concentration dependence of the $Na^+$ and $Cl^-$ contents per ionic unit of DNA in the DNA−DDA complex. Three regions A, B, and C partitioned by two vertical dotted lines are the undulated lamella, transition lamella, and ordinary lamella regimes.

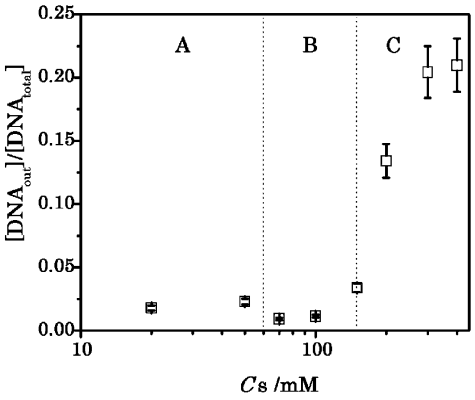


**Figure 9.** Salt concentration dependence of DNA amount diffusing from the DNA−DDA complex to the NaCl solution equilibrating with the complex. Three regions A, B, and C partitioned by two vertical dotted lines are the undulated lamella, transition lamella, and ordinary lamella regimes.

with $C_s$ in the defect hexagonal and ordinary hexagonal regimes, but it is invariant with $C_s$ and relatively small in the transition regime. The concentration of DNA in the solution phase equilibrating with the complex is considered a critical DNA concentration for the complexation of DNA with OTAC, $CCC^{DNA}_{DNA-OTA}$. The result shown in Figure 7 indicates that the $CCC^{DNA}_{DNA-OTA}$ increases with $C_s$ in the defect hexagonal and ordinary hexagonal regimes but is invariant with $C_s$.

Figure 8 shows ratios of $Na^+$ and $Cl^-$ amounts to an ionic unit of DNA in the DNA−DDA complex equilibrated with the NaCl solution, $N_{Na^+}/N_{DNA}$ and $N_{Cl^-}/N_{DNA}$ as functions of $C_s$. An excess amount of $Cl^-$ over $Na^+$ in the complex is more than 0.25 per ionic unit of DNA of the complex. The composition ratio of DDA molecule to ionic unit of DNA molecule in the complex is more than 1.25 judging from the electrical neutrality condition of the complex. Figure 8 shows that the amounts of $Na^+$ and $Cl^-$ ions in the complex increase with $C_s$ in the ordinary lamella regime.

A small amount of DNA molecules diffuse from the DNA−DDA complex into the NaCl solution phase. Figure 9 shows a diffusing amount of DNA molecules from the complex to the NaCl solution, $([DNA^{out}] \times V_{NaCl})/(N_{DNA} + [DNA^{out}] \times V_{NaCl})$ as a function of $C_s$. The diffusing amount of DNA is invariant with $C_s$ in the undulated lamella and transition regimes, but it increases with an increase of $C_s$ in the ordinary lamella regime. The critical DNA concentration for the complexation of DNA with DDA, $CCC^{DNA}_{DNA-DDA}$ increases with the increase of $C_s$ in the ordinary lamella regime, but is invariant with $C_s$ and relatively small in the undulated lamella and transition regimes.

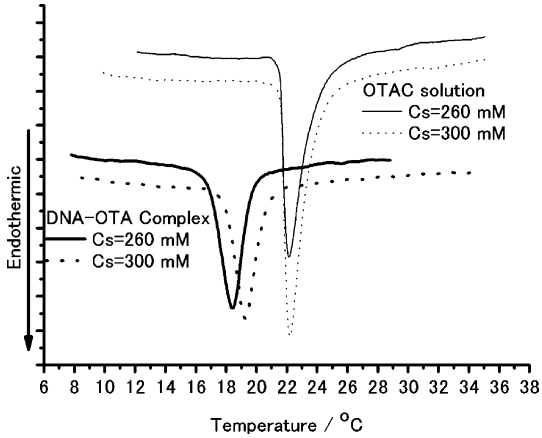


**Figure 10.** DSC curves of DNA−OTA complex equilibrating with the NaCl solution (thick lines) and OTAC solution (thin lines) at $C_s = 260$ mM (solid lines) and 300 mM (dotted lines).

**Table 2.** Transition Enthalpy $\Delta H$ and Transition Temperature of DNA−OTA Complex and OTAC Solution Obtained from the DSC Measurement

| | DNA−OTA complex | | OTA solution | |
|---|---|---|---|---|
| $C_s$/mM | $T_K$/°C | $\Delta H$/kJ mol$^{-1}$ | $T_K$/°C | $\Delta H$/kJ mol$^{-1}$ |
| 260 | 16.9 | $12 \pm 3$ | 21.6 | $20 \pm 3$ |
| 300 | 17.9 | $13 \pm 3$ | 21.6 | $25 \pm 3$ |

**3.3. Thermal Behavior of the Complex.** Figure 10 shows the DSC curves of the DNA−OTA complex equilibrating with the NaCl aqueous solution. The measurements of DSC were made for the DNA−OTA complexes at $C_s = 10$, 100, 260, and 300 mM and the DNA−DDA complexes at $C_s = 10$, 100, and 300 mM. It is very interesting to find out that the DNA−OTA complexes at $C_s = 260$ and 300 mM exhibit the endothermic peaks as seen in Figure 10, but others do not. It is well-known that the Krafft transition of the surfactant molecule is endothermic.[20] The endothermic peaks observed for the OTAC solutions at $C_s = 260$ and 300 mM are also shown in Figure 10 for comparison. The transition temperature of the DNA−OTA complex is lower than that of OTAC solutions. The transition enthalpies per 1 mol of surfactant molecule of the DNA−OTA complex and OTAC solutions obtained from the DSC curves are shown in Table 2. It is noticeable that the transition enthalpy of the DNA−OTA complex is about half of that of the OTAC solution.

## 4. Discussions

The possible ordered structures emerging the SAXS profiles observed for the DNA−OTA complexes in the ordinary hexagonal regime and the defect hexagonal regime, respectively, are schematically depicted in Figure 11a (the ordinary hexagonal structure) and b (the defect hexagonal structure). The arrays of the surfactant micelle and DNA need to make the same hexagonal planes for the scattering peaks with the spacing ratio of $1:3^{1/2}:2$. The hexagonal lattices of columned surfactant micelle and DNA shown in Figure 11a have the same scattering hexagonal planes. The hexagonal column of DNA-inverted surfactant shown in Figure 1 can explain the scattering peaks with the spacing ratio of $1:3^{1/2}:2$ but cannot explain both of the peaks with the spacing ratio of $1:3^{1/2}$ and the increase in $d$ with $C_s$ shown in Figure 2b. The 1:1 complex of a phosphate group of DNA and a surfactant molecule at the low $C_s$ favors a site-binding model leading to the DNA-inverted surfactant. The

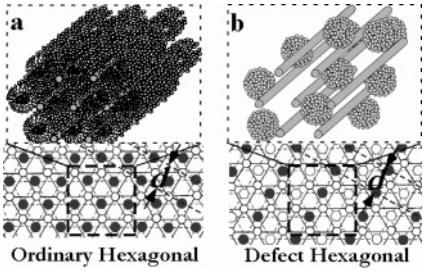


**Figure 11.** Possible schematic models of ordinary 2D hexagonal structure (a) and defect 2D hexagonal structure (b) of the DNA−OTA complex. The dark and small open circles, respectively, represent the surfactant micelle and DNA, and the large open circles shown in (b) are vacancy sites. The planes for inducing the first scattering peak are represented by dark and broken lines. The arrows indicate the lattice spacing, $d$. The 3D structures in the lattice domains surrounded by the thick broken lines are depicted in the upper figures. The ordinary hexagonal lattices of surfactant micelle and DNA shown in (a) have the same scattering planes that induce the peaks at $q$ values, the ratio of which is $1:3^{1/2}:2$. The ordered planes, the distance between which is half of $d$, are missing in the array of spheroidal micelles located at sites represented by dark circles shown in (b) and annihilate the third peak observed in the SAXS profile of the ordinary hexagonal lattice.

SAXS profiles missing the third peak, however, inevitably lead to abandoning the DNA-inverted surfactant model for the DNA−OTA complex. In the defect hexagonal lattice, a miss of the scattering planes at an interval of $^1/_2d$ leads to the annihilation of the third scattering peak. That is, the defect hexagonal lattice induces the scattering peaks with the spacing ratio of $1:3^{1/2}$. The OTA micelle formed in the ordinary hexagonal regime is rodlike. The micelle in the defect hexagonal regime might be spheroid. The spheroidal micelles might occupy the lattice sites represented by the dark circles but not the sites represented by the large and open circles on one plane perpendicular to the hexagonal column shown in Figure 11b. The defect of the hexagonal columns of micelles arrayed in an alternative manner shown in Figure 11b can annihilate the scattering planes, a distance between which is half of $d$, and the third peak scattered from the ordinary hexagonal lattice shown in Figure 11a. It should be mentioned that the hexagonal structure of DNA surrounded with the inverted surfactant shown in Figure 1 is possible in the ordinary hexagonal regime. The increase of $d$ with $C_s$ shown in Figure 2b should lead to an increase of the parameter of disorder, $\Delta/d$, because of increasing the space for DNA to move with the increase of $d$ in the case mentioned above. The experimental result is, however, opposite as shown in Figure 2b. The decrease of $\Delta/d$ should be explained by lengthening the cylindrical micelle with $C_s$, which stabilizes the structure of ordinary hexagonal lattice shown in Figure 11a. The inverted surfactant hexagonal structure shown in Figure 1 cannot be adapted to the $C_s$-dependent structure described above.

The change from the defect hexagonal structure at low $C_s$ to the ordinary hexagonal structure at low $C_s$ is made in order to lower the electrostatic interaction energy. Roles of the electrostatic interaction are essential in making the complex of DNA with surfactant molecules. The architecture of the DNA−surfactant complex is regulated in order to lower the electrostatic energy that is a function of spatial distribution of charged entities, phosphate group of DNA, surface charges of micelles, and salt ions. The aggregate of surfactant OTA is expected to form cylindrical micelle in the DNA−OTA complex, since the micelle of OTA with a C18 alkyl chain is cylindrical in the aqueous solution. In arraying columnar DNA and cylindrical OTA micelles in an alternative manner, the gap between line charge densities of DNA and cylindrical micelles leads to the

high electrostatic interaction energy of the complex. A line density of DNA ($\lambda_{DNA} = 5.88\ nm^{-1}$) is much smaller than that of the OTA cylindrical micelle ($\sigma_{OTA} = 24-35\ nm^{-1}$), which is estimated from the relation $\sigma_{OTA} = 2\pi l_{OTA}/s_{OTA}$ where $l_{OTA}$ and $s_{OTA}$, respectively, are a length of stretched OTA molecule ($\sim 0.15 + 0.127 \times 18 = 2.4$ nm)[21] and an area of the micelle surface occupied by one OTA molecule. Here, $s_{OTA}$ can be obtained from the shape factor relation: $v_{OTA}/s_{OTA}l_{OTA} = {}^1/_3-{}^1/_2$ for the cylindrical micelle,[22] where $v_{OTA}$ is a volume of OTA molecule ($\sim 0.0274 + 0.0269 \times 18 = 0.512\ nm^3$).[21] The 2D hexagonal packing of the DNA and OTA cylindrical micelle shown in Figure 11a is unstable because of the high electrostatic energy of the complex unless the salt molecules do not effectively shield the electrostatic interaction. The salt molecules are penetrating into the complex in the transition regime as indicated by Figure 6. The electrostatic interaction due to the charge density gap mentioned above can be shielded in the salt solution at $C_s$ above 250 mM. For keeping the local neutrality condition of electricity at the low $C_s$, the shape of micelle in the DNA−OTA complex is forced to be spheroid. The spheroid ionic micelle can balance to the charge density of DNA by less dense distribution among the DNA columns. The defective 2D hexagonal array of the spheroids as shown in Figure 11b can satisfy the local neutrality condition. Therefore, the defective 2D hexagonal array is observed in the SAXS profiles as shown in Figure 2a at $C_s$ below 150 mM.

The free energy of the cylindrical OTAC micelle is lower than that of the spheroid in the solution phase because of the lengthy alkyl chain. So is the OTA micelle in the DNA−OTA complex. Therefore, the free energy of the defective hexagonal complex consisting of the spheroid micelle is higher than that of the ordinary hexagonal complex consisting of the cylindrical micelle. The chemical potential of the DNA molecule in the complex, $\mu_{DNA}$, is given as $\mu_{DNA} = \mu^0_{DNA} + T \ln CCC^{DNA}_{DNA-OTA}$ at the equilibrium, where $\mu^0_{DNA}$ and $T$, respectively, are a standard chemical potential of DNA and the Boltzmann temperature. The smaller $CCC^{DNA}_{DNA-OTA}$ is accompanied by the more stabilized complex or the lower $\mu_{DNA}$. The transitional decrease of $CCC^{DNA}_{DNA-OTA}$ from the defect hexagonal regime to the transition regime as shown in Figure 7 reflects on the transitional decrease in the free energy of the complex with the regime change. This is possibly induced by the low free energy of coexisting cylindrical micelles in the complex. It should be mentioned that cylindrical micelles lead to more compaction of DNA than the spheroidal micelles as indicated by Table 1. The compaction also contributes to decreased $\mu_{DNA}$. The amounts of $Na^+$ and $Cl^-$ ions provided from the solution phase control the degree of transition from the phase consisting of spheroidal micelles to the phase composed of cylindrical micelles. The increase of small ions in the DNA−OTA complex with $C_s$ as shown in Figure 6 is accompanied by the increase in the relative SAXS intensity emerging from the latter phase as shown in Figure 3. The present experiment cannot, however, reveal how distributed $Na^+$ and $Cl^-$ ions are. It is inferred that $Na^+$ and $Cl^-$ ions, respectively, are more distributed into the spheroidal micelle-rich phase and the cylindrical micelle-rich phase.

Is the structural difference of the micelles in the complex described above consistent with the fact that the endothermic DSC peaks are observed for the DNA−OTA complexes in the ordinary hexagonal regime but not for the complexes in the defect hexagonal regime? It is well-known that the ionic surfactant micelles suspended in water at a temperature above the Krafft temperature, $T_K$, transform to the hydrated solid or crystal at a temperature below $T_K$.[23] The strong attraction between long alkyl chains makes them array in a parallel manner to stabilize the all-trans chain of their ordered array in the surfactant aggregate. The OTAC aggregates form the lamella structures in the solution at a temperature below $T_K$. In the solution phase, the stacking freedom of alkyl chains is of two dimensions. The alkyl chains in cylindrical micelles can also stack in one dimension along a long axis of the cylinder. The fact that a transition enthalpy of the DNA−OTA complex per 1 M OTA is about half of that of the OTAC shown in Table 2 can be explained by the difference in the stacking dimensionality between the complex (1D) and the solution (2D). When the alkyl chains in the cylindrical micelles are stacking at a temperature below the transition temperature observed in the DSC measurements, nanostructures of the complex should change accordingly. To examine the structural change with the temperature, the SAXS measurements for the DNA−OTA complex were made by raising the temperature from 10.8 to 26.3 °C. Figure 12 shows the temperature dependence of the SAXS profiles of the DNA−OTA complex in the 260 mM NaCl solution, the lattice spacing, $d$, and the parameter of disorder, $\Delta/d$, obtained from the profiles. Peaks characteristic of the ordinary hexagonal structure are always observed, and $d$ transitionally decreases from 5.45 to 5.15 nm at the transition temperature, $T_K$. The change in $d$ with the transition is due to

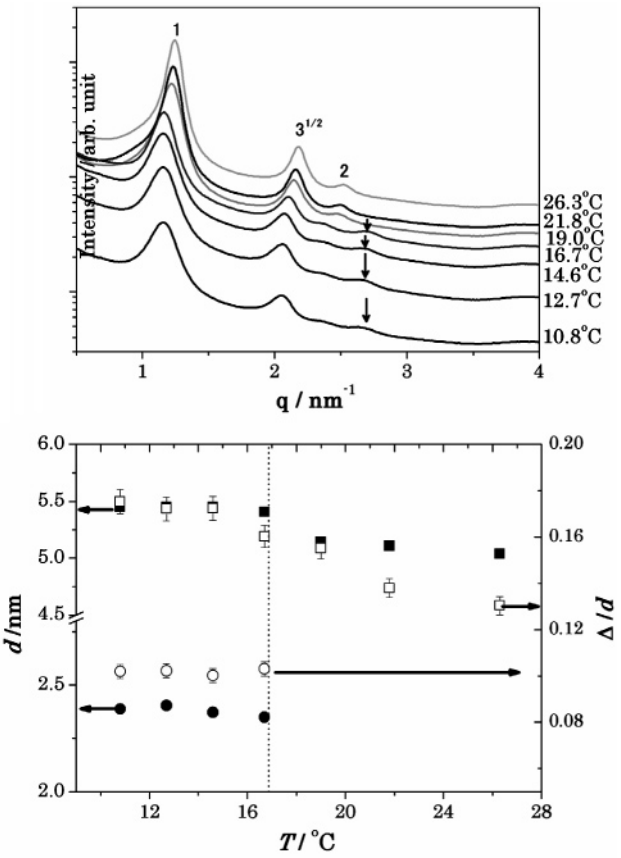


**Figure 12.** Temperature dependence of the SAXS profiles of the DNA−OTA complex in the 260 mM NaCl solution (a), and the lattice spacing, $d$, and the parameter of disorder, $\Delta/d$, obtained from the profiles (b). (a) Peaks with spacing ratio of $1:3^{1/2}:2$ are observed. Peaks at $q \approx 2.7$ appear at temperature below 16.7 °C and disappear at temperature above 19.0 °C. (b) The closed and open symbols, respectively, represent $d$ and $\Delta/d$. The symbols of square and circle, respectively, represent the data corresponding to the first peak and the peak at $q \approx 2.7$. A dotted vertical line in (b) represents the transition temperature ($T_k = 16.9$ °C) observed in the DSC measurement for the DNA−OTA complex in the 260 mM NaCl solution.

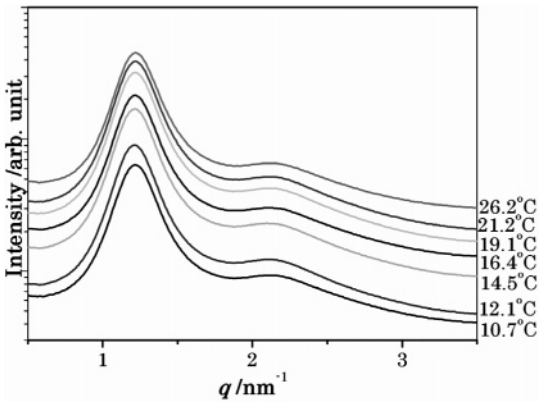


**Figure 13.** Temperature dependence of the SAXS profiles of the DNA-OTA complex equilibrated with 20 mM NaCl solution. Broad peaks with a spacing ratio $1:3^{1/2}$ are observed.

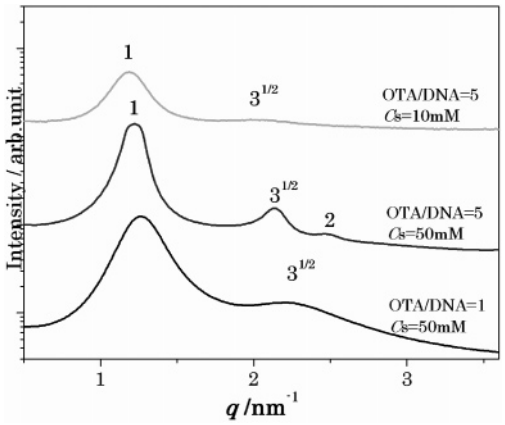


**Figure 14.** SAXS profiles of DNA−OTA complexes at different charge molar ratios of OTA/DNA in the NaCl solutions at $C_s = 50$ and 10 mM.

a change in the radius of cylindrical micelle, $r_{cyl}$, which increases with a fraction of the trans configuration in the alkyl chain. The transitional change in $d$ reflects on the transitional change in the fraction of the trans configuration in the alkyl chain at $T_K$. The trans configuration is most favored in the stacking state of the alkyl chain, which lengthens $r_{cyl}$ and $d$.

The fourth peak at $q \approx 2.6$ appearing at temperature below 16.7 °C, as shown in Figure 12a, cannot be identified with the $\sqrt{7}$ peak scattered from the 2D hexagonal lattice plane, and it disappears at temperature above 19.0 °C. It is obvious that the structure of the DNA−OTA complex changes at the transition temperature ($T_K = 16.9$ °C) observed in the DSC measurement. The form factor of a cylinder with a radius $r_{cyl}$, which is proportional to $\int_0^{\pi/2} d\phi[J_1(qr_{cyl} \sin \phi)/qr_{cyl} \sin \phi]^2 \sin \phi$ where $J_1(x)$ is the first-order Bessel function,[24] shows the first peak at $q = 5.0/r_{cyl}$ according to our numerical calculation. The fourth peaks at $q \approx 2.7$ can be identified with a form factor of the cylinder with $r_{cyl} = 1.9 \pm 0.1$ nm, which is compatible with the fully stretched alkyl length of OTA, 2.25 nm. It should be mentioned that the SXAS profiles of the DNA−OTA complex at $C_s = 300$ mM change in the same way as described above at the transition temperature ($T_K = 17.9$ °C) observed in the DSC measurement for the DNA−OTA complex in the 300 mM NaCl solution. The temperature-dependent SAXS profiles described above strongly suggest that the micelle in the DNA−OTA complex in the ordinary hexagonal regime is cylindrical.

The Krafft transition cannot be observed for the spheroid micelle in the DNA−OTA complex in the defect Hexagonal regime because the alkyl chains in the spheroid cannot geometrically array in a parallel manner to stack with each other. No Krafft transition might lead to little structural change of the complex with temperature. To examine this, the SAXS measurements were made for the DNA−OTA complexes equilibrated with the 20, 50, and 100 mM NaCl solutions. The obtained SAXS profiles at $C_s = 20$ mM are shown in Figure 13. Broad peaks with a spacing ratio of $1:3^{1/2}$ are observed at temperatures between 10.7 and 26.2 °C. This confirms no structural change with no Krafft transition.

It is well-known that the energy reduction due to the van der Waals attraction between alkyl chains of the surfactant molecules in the bulk solution exceeds their thermally agitating energy at the temperature below the Krafft temperature. The endothermic transition observed for the DNA−OTA complex corresponds to the Krafft transition, that is, the order−disorder transition of alkyl chain of the OTA molecule. It is also known that the Krafft transition temperature of the surfactant aqueous solution increases with an increase in the salt concentration.[25] According to the thermodynamics, the transition temperature, $T_K$, is given by the relation, $\Delta H = T_K \Delta S$, where $\Delta H$ and $\Delta S$, respectively, are changes of enthalpy and entropy with the transition. The stacking of alkyl chains in an ordered manner is accompanied with counterion binding and dehydration of the headgroup of the surfactant molecule. An increase in $C_s$ has the effect of reducing the contribution of counterion binding and dehydration to $\Delta S$, because the changing amounts of binding counterion and dehydrating water molecules decrease with $C_s$. The $\Delta H$ due to van der Waals attraction between the alkyl chains is independent of $C_s$. Thus, $T_K$ of the OTAC micelle in the solution increases with $C_s$. This is also the case for cylindrical micelles in the DNA−OTA complex at $C_s$ above 260 mM as shown in Figure 10. The transition temperatures, $T_K$, of the DNA−OTA complexes at $C_s = 260$ and 300 mM, respectively, are 16.9 and 17.9 °C. It is worthwhile to point out that the entropy change, $\Delta S$, with the Krafft transition of the DNA−OTA complex, 41 J mol$^{-1}$ $T^{-1}$ at $C_s = 260$ mM and 44 J mol$^{-1}$ $T^{-1}$ at $C_s = 300$ mM are much smaller than that of OTAC in the solution phase, at 67 J mol$^{-1}$ $T^{-1}$ at $C_s = 260$ mM and 84 J mol$^{-1}$ $T^{-1}$ at $C_s = 300$ mM. This reflects on stronger electrostatic constrained force exerting on the micelles in the DNA−OTA complex than that in the solution phase.

The structure shown in Figure 11a, which needs more OTA molecules than 1 for an ionic unit of DNA, can be stabilized by an increase of the OTA content in the DNA−OTA complex.[6] To examine the stabilizing effect of the increase of the OTA, the SAXS profiles of the DNA−OTA complex at $C_s = 50$ and 10 mM were measured with change of the charge molar ratio of OTA to DNA in the complex, OTA/DNA. Figure 14 shows the SAXS profiles of DNA−OTA complexes which demonstrate the transformation of the defect hexagonal structure at OTA/DNA = 1 into the ordinary hexagonal structure at OTA/DNA = 5 in the NaCl solution at $C_s = 50$ mM, but in the NaCl solution at $C_s = 10$ mM, no transformation of the defect hexagonal structure takes place at OTA/DNA = 5. The important role of electrostatic shielding effect of salt in the structure of the DNA−surfactant complex also takes place in this experiment.

As described in the Results section, the experimentally obtained $\rho$ value of the DNA−DDA complex is $1.25 \pm 0.06$ in the salt-free system. The obtained $\rho$-value provides with a shape factor or a packing parameter of bilayer as follows. The surface charge density of the DNA array sandwiched between DDA bilayer, $\sigma^0_{DNA}$, is 2.16 nm$^{-2}$, which is obtained from the relation $\sigma^0_{DNA} = \lambda_{DNA}/d^0_{DNA}$ where $d^0_{DNA}$ is an inter-DNA

distance in the DNA−DDA complex in a salt-free system obtained from the SAXS profiles shown in Figure 4a. The sum of anionic charges of DNA and $Cl^-$ should be balanced with the cationic charge of the DDA bilayer with the surface density, $\sigma_{DDA}$ ($= \rho \cdot \sigma^0_{DNA}/2$), which is estimated to be $1.32 \pm 0.07$ $nm^{-2}$. The area of bilayer surface occupied by one DDA molecule, $s_{DDA}$, can be estimated from $s_{DDA} = 1/\sigma_{DDA}$. The length of DDA molecule in the bilayer is $0.7 \times l_{DDA}$,[26] where $l_{DDA}$ is the contour length of the stretched DDA molecule ($0.154 + 0.126 \times 12 - 1.67$ nm). The volume of the DDA molecule, $v_{DDA}$, is estimated as 0.700 $nm^3$ ($\sim 0.0274 \times 2 + 0.0269 \times 24$).[21] Then, the shape factor, $v_{DDA}/(s_{DDA} \cdot 0.7 l_{DDA})$ is $0.79 \pm 0.04$, which is consistent with the value of the shape factor of $^1/_2-1$ for the bilayer.[22] The value of 0.79 of the shape factor is smaller than 1, that is, an ideal shape factor for the flat bilayer. This indicates that the undulated bilayer shown in Figure 5a might be favored in the salt-free condition. There might be other possible explanations than that described above. The excess of $Cl^-$ could be alternatively explained by assuming about 25% DDA molecules adhering onto the already occupied DDA on the backbone of the DNA polymer through the hydrophobic effect. If this is the case, the structural change with $C_s$ as indicated by Figure 4 is not realized because of little penetration room for the water molecules into the complex structure mentioned above. The mechanical and dielectric relaxation measurements of the complexes could provide useful information[12] for solving the rather speculative discussion described above.

It should be mentioned that the complex made from DNA mixed with the chloride salt of the surfactant in the NaCl aqueous solution led to the same results as those at the high $C_s$ in the present experiment. This means that the structures of DNA−surfactant complexes at high $C_s$ are not greatly affected by the production procedure.

## 5. Conclusions

The SAXS profiles obtained for the DNA−surfactant complexes such as DNA−OTA and DNA−DDA revealed that the nanostructures change with the NaCl concentration of the solution equilibrating with the complex. The structure of the DNA−OTA complex transforms from the defective 2D hexagonal structure consisting of columnar DNA surrounded by the spheroid micelles to the ordinary 2D hexagonal columnar structure of DNA and cylindrical micelle with an increase in the NaCl concentration from 150 to 260 mM. The SAXS profiles scattered from the former and latter structures, respectively, exhibit two peaks with a spacing ratio of $1:3^{1/2}$ and three peaks with a spacing ratio of $1:3^{1/2}:2$. The Krafft transition is observed for the latter structure but not for the former structure in the differential scanning calorimetry. Contents of $Na^+$ and $Cl^-$ ions in the complexes evaluated from the atomic absorbance for $Na^+$ and the potentiometry for $Cl^-$ demonstrate charge molar ratios of OTA/DNA = 1 and DDA/DNA = 1.25. Molar ratios of $Na^+$ and $Cl^-$ ions to an ionic unit of DNA molecule in the DNA−OTA complex equilibrated with the NaCl solution at the concentration below 100 mM are much less than 0.1, while they increase with increase of the concentration above 200 mM.

**Acknowledgment.** This work is supported by a Grant-in Aid for Scientific Research (B) (no. 16350128) from the Ministry of Education, Science, Sports and Culture of Japan. The SAXS experiments were performed at SPring 8 with the approval of Japan Synchrotron Radiation Institute.

## References and Notes

(1) Safinya, C. R.; Addadi, L. *Curr. Opin. Solid State Mater. Sci.* **1996**, *1*, 387.
(2) Bloomfield, V. A. *Biopolymers* **1997**, *44*, 269−282.
(3) Wilson, R. W.; Bloomfield, V. A. *Biochemistry* **1979**, *18*, 2192−2196.
(4) Bloomfield, V. A. *Curr. Opin. Struct. Biol.* **1996**, *6*, 334−343.
(5) Pelta, J.; Livolant, F.; Sikorav, J. L. *J. Biol. Chem.* **1996**, *271*, 5656−5666.
(6) Zhou, S.; Liang, D.; Burger, C.; Yeh, F.; Chu B. *Biomacromolecules* **2004**, *5*, 1256−1261.
(7) Mel'nikov, S. M.; Sergeyev, V. G.; Yoshikawa, K.; Takahashi, H.; Hatta, I. *J. Chem. Phys.* **1997**, *107*, 6917−6924.
(8) Lasic, D. D.; Strey, H.; Stuart, M. C. A.; Podgonik, R.; Frederik, P. M. *J. Am. Chem. Soc.* **1997**, *119*, 832−833.
(9) Rädler, J. O.; Koltover, I.; Salditt, T.; Safinya, C. R. *Science* **1997**, *275*, 810.
(10) Koltover, I.; Salditt, T.; Safinya, C. R. *Biophys. J.* **1999**, *77*, 915−924.
(11) Sasaki, S.; Koga, S. *Macromolecules* **2004**, *37*, 3809−3814.
(12) Antonietti, M.; Neese, M. *Langmuir* **1996**, *12*, 4436−4441.
(13) Thûnemann, A. F. *Prog. Polym. Sci.* **2002**, *27*, 1473−1572.
(14) Antonietti, M.; Conrad, J.; Thûnemann, A. *Macromolecules* **1994**, *27*, 6007−6011.
(15) Ghirlando, R.; Wachtel, E. J.; Arad, T.; Minskey, A. *Biochemisrty* **1992**, *31*, 7110.
(16) Salditt, T.; Koltover, J.; Rädler J. O.; Safinya, C. R. *Phys. Rev. E* **1998**, *58*, 889.
(17) Klevens, H. B. *J. Am. Oil Chem. Soc.* **1953**, *30*, 74.
(18) Lang, J. *J. Phys. Chem.* **1982**, *86*, 992.
(19) Vainshtein, B. K. *Diffraction of X-ray by Chain Molecules*; Elsevier: New York, 1996; Chapter 5.
(20) Kodama, M.; Tsujii, K.; Seki, S. *J. Phys. Chem.* **1990**, *94*, 815−819.
(21) Tanford, C. *The Hydrophobic Effect*; Wiley: New York, 1973.
(22) Islaelachivili, J. *Intermolecular and Surface Forces*; Academic Press: London, 1992.
(23) Shinoda, K. *Colloidal Surfactants*; Academic Press: New York, 1963.
(24) Guinier, A.; Fournet, G. *Small angle scattering of X-rays*; John Wiley and Sons: New York, 1955.
(25) Vautier-Giongo, C.; Bales, B. L. *J. Phys. Chem. B* **2003**, *107*, 5398−5403.
(26) Gruen, D. W. R.; De Lacey, E. H. B. *Surfactant in Solution*; Mittal, K. L., Lindman, B., Eds.; Plenum: New York, 1984.

BM060059J